6. Thermal Remote Sensing Methods in Landscape Ecology

Jeffrey C. Luvall and H. Richard Holbo

6.1 Introduction

Plant ecologists are well acquainted with the importance of the microclimate in governing physiological processes. Temperature plays a fundamental and often limiting role in many biological processes through its control of the rate of biological-chemical reactions, i.e., Q_{10}. Because plants are poikilothermic, their temperatures are closely linked to thermal energy exchanges with the microclimate. Evaluating these energy exchanges to improve our understanding of the interdependencies between plants and their microclimates for various types of landscape vegetations is not a simple task. For example, in a forested landscape, the upper leaves of the canopy receive high levels of solar radiation and dissipate the resulting heat while maintaining leaf temperatures within a fairly narrow range, if a survivable balance between photosynthesis and respiration is to exist. In addition, the presence of a forest canopy is known to moderate the physical microclimate of all associated plant communities.

It is recognized that canopy and leaf temperatures are controlled by a combination of thermal energy fluxes and vegetation-dependent or site-specific factors. We know that the amount of solar radiation received by the forest canopy has a major influence on all other thermal energy fluxes in the forest canopy and thus on leaf temperatures. Although the microclimate of the canopy is influenced by prevailing regional weather conditions, during clear weather the amount of solar radiation received is more strongly influenced by the local topography and land manage-

ment practices. Among the many site-specific factors that contribute to canopy temperature are leaf and canopy morphology, species composition, and water status. Perhaps not so surprisingly, air temperature is often a poor predictor of leaf temperature, especially when air temperature is measured by using traditional meterological shelters in different parts of the landscape.

We may expect that the structural and physiological variability that characterizes forests, in contrast to those of other landscape types like prairies and shrublands, leads to a wide range of small microclimates within a forest. In fact, the complexity of the forest canopy, the volume it occupies, stomatal controls over water loss, and the distances separating tree crowns from the soil below all interact to produce thermal energy budgets that are dramatically different from those typical of shorter vegetations or crops. For even a seemingly uniform forest type, vertical differences in leaf and air temperatures within the canopy, variations in depth of the forest canopy, leaf area index, and the crown topographies operate to preclude a generalized summary about its microclimate across the lateral extent of forested landscapes. Many forests occur in mountainous areas, adding further complications because of elevational differences, topography, highly variable soil moisture availabilities, and diversity of forest community types.

Forest edges constitute yet another source of variability, further generating complex microclimate gradients. Ultimately, the physical environments at such edges support the many interesting and dynamic associations of woody and herbaceous species characteristic of forest plant communities (Ranny et al. 1981). Nonetheless, these edges complicate the micrometeorological picture excessively, and measurements across them, which are needed to define the nature of spatial variability in forest edge microclimates and energy budgets, are generally lacking (e.g., Miller 1975; Thistle et al. 1987).

In landscape ecology both the technological means and a corresponding analytical rationale are needed to gain more information about microclimatic processes at scales which can be extended over large areas to interpret the vegetation patterns observed. For microclimatological analyses, traditional techniques of determining leaf and/or canopy temperatures have had to rely on the use of small thermocouples or hand-held infrared thermometers. The few measurements that may be taken with these techniques necessarily provide a very small sampling of the overall landscape. Practical constraints usually limit the number of samples that can be acquired across a landscape to far less than a reasonable number. But now, because of recent developments in thermal remote sensing techniques, there is a feasible way to quantitatively assess relatively small-scale microclimatic patterns and then evaluate them with respect to the larger patterns of landscape elements. Thermal remote sensing instruments are available to measure temperatures over fairly large areas at snapshot speeds.

In his article "Landscape Ecology: State of the Art," Risser (1987) appealed for new techniques designed to address specific questions concerning landscape structure and function. Accordingly, we propose that thermal remote sensing of forest canopy temperatures is such a technique and that methodologies can be derived from it to analyze the thermal functions of landscape structures and lead toward

a better understanding of pattern and process in landscape ecology. In this chapter we address the topic of applying forest canopy temperatures to landscape ecology by posing these questions:

1. What are the relationships between temperature and energy budgets of forest canopies?
2. What techniques are available to measure canopy temperatures at landscape spatial scales?
3. Can our understanding of forest function and structure be improved by having landscape-scale measures of spatial variability in forest canopy temperatures and thermal response?

6.2 Flow of Thermal Energy Across Forested Landscapes

The heterogeneity of forests across the landscape results in a spatial discontinuity of microclimates. Distinct differences in air temperature and humidity are created by the forest canopy in response to the environment. As a result, horizontal transfers of energy occur between adjacent forest canopies. These lateral exchanges of energy are termed "advection."

Advective effects in forests may be grouped into three general types (Oke 1987). One type, the "clothesline effect," occurs along the edges of dissimilar vegetation types. The term *clothesline effect* describes the condition when a flow of dry air leaves a moisture-limited surface, such as a clearing, and enters the forest. Responding to the lower humidity, evapotranspiration rates temporarily increase, soil moisture is reduced, and a drier microclimate results. The counterpart to the "clothesline effect" is an advective condition called the "oasis effect." The *oasis effect* describes a situation wherein a flow of dry air passes over a moisture-unlimited surface. Because surface moisture is unlimited, evapotranspiration increases at the expense of heat energy from the air, resulting in lower temperatures and higher humidities. The third type of advective effect, accompanying either "clothesline" or "oasis" processes, is the concept of "fetch." Fetch is an index to the thickness of the layer of air in contact with a surface that is in equilibrium with the energy exchanges occurring at the surface. Typical thicknesses for equilibrium surface layers range from 20 cm for smooth desert surfaces with an inversion to 200 m or more for forests. The properties of a moving air mass at the leading edge of a new surface obviously represent the old surface it has just passed over, and it takes some distance before a new boundary layer forms that is fully in balance with the energy exchanges occurring at the new surface. The distance that the air must travel before it achieves such an equilibrium throughout a specified thickness is called fetch. Fetch is an important consideration, primarily when making micrometeorological estimates of surface thermal energy exchanges. The practical consequence of fetch is to emphasize the point that micrometeorological instrumentation must be positioned within this equilibrium layer. Otherwise, energy exchange estimates will be in error because the measurements will have inadvertently sampled properties representative of upwind sur-

faces. Depending on the type of surface, atmospheric stability, prevailing wind speeds, and the deployment height of the micrometeorological instruments, required fetch distances can exceed several hundred meters. These considerations make it virtually impossible to select micrometeorological measurement sites free of the potential effects of edge discontinuities.

6.3 Surface Energy and Radiation Budgets

In spite of the micrometeorological limitations of advection, which complicate the choices of sites, it has proven useful to model in thermal energy budget terms energy exchanges occurring at surfaces. The energy budget provides a framework for comparing microclimates in ways that cannot be accomplished by using other formulations involving environmental variables (e.g., temperature, humidity, wind speed, and solar radiation). By translating these variables into the components of an energy budget, all types of landscape surfaces from vegetated (forest and herbaceous) to nonvegetated (bare soil, roads, and buildings) may be compared. The units normally used to express these energies are watts per square meter (Wm^{-2}) to describe the rates of energy flow and joules per square meter (Jm^{-2}) to quantify the total amounts of energy accumulated over time.

We begin a brief review of the thermal energy budget of forests by first considering the radiation fluxes acting upon the surface, the residual of which results in the net radiation flux, Q^*. Then, the nonradiative terms of the energy budget are discussed, the sum of which must equal Q^*. Although the discussion emphasizes forests, the principles apply to surfaces of all types. For a comprehensive discussion of the thermal energy budgets, the reader may consult the excellent text by Oke (1987).

The net all-wave radiation balance, Q^*, of forest canopies may be defined by considering its shortwave (or solar) and long-wave radiation components separately. This compartmented approach helps focus on areas where remote sensing techniques are applicable.

The net flux of solar radiation, K^*, can be found from

$$K^* = (1 - \alpha)\, \phi\, K\downarrow \tag{6.1}$$

where α = surface albedo = $K\uparrow/K\downarrow$, ϕ = a surface slope and aspect solar gain coefficient, $K\downarrow$ = incoming solar radiation, and $K\uparrow$ = outgoing (reflected) solar radiation.

The surface angle dependency, ϕ (Garnier and Ohmura 1968), is sometimes left out of the equation when the surface in question is assumed to be essentially flat, as an entire landscape might appear to be. However, while ϕ is usually not large (<1.2), it takes on increasing importance as short-term observations are made and as spatial resolution is improved. Its influence can often explain much of the variability in thermal image data.

The net flux of long-wave radiation at the surface, L , is

$$L^* = L\downarrow - L\uparrow \tag{6.2}$$

where $L\downarrow$ = incoming long-wave radiation from the atmosphere, and $L\uparrow$ = outgoing long-wave radiation emitted from the surface.

The long-wave radiation emitted from a surface is the variable measured by using thermal remote sensing. It is a function of surface temperature:

$$L\uparrow = \varepsilon \sigma T_s^4 \tag{6.3}$$

where ε = emissivity, σ = Stefan-Boltzman constant ($5.7 \times 10^{-8} Wm^{-2}T^{-4}$), and T_s = surface temperature (Kelvin).

The net flux of all-wave radiation, Q^*, is the sum of Eqs. 6.1 and 6.2:

$$Q^* = K^* + L^* \tag{6.4}$$

Net radiation (Q^*) is a very important term because it represents the amount of energy available at the surface for partitioning into the nonradiative processes, LE, H, and G, of the thermal energy budget:

$$Q^* = LE + H + G \tag{6.5}$$

where LE = latent heat exchange, or evapotranspiration (ET), H = sensible heat exchange into the atmosphere, and G = conduction heat exchange with biomass and soil.

For a typical daytime situation during fair summer weather, Q^* will be the heat energy source, except for short periods following shading by clouds. For coniferous forests, Q^* may be about 65% of $K\downarrow$, proportionally lower for deserts, and higher for well-watered crops. LE and H are the largest dissipative energy fluxes. But it would be ill-advised to assume that LE is predominant. Coniferous canopies can exchange an amount equal to Q^* by H alone, without large increases in needle temperatures. The magnitude of G is usually small; however, during brief periods near sunrise or sunset, it may become disproportionately large.

These approximations aside, the partitioning of the terms in the energy budget depends on a great many surface characteristics. In forested landscapes, the proportioning of the surface energy budget terms depends largely on forest type and moisture conditions. Forest types that exhibit distinct energy budgets will likely have differences in plant community types, canopy biomass, or leaf area index. Moisture conditions encompass a number of factors, including phenological status, and thus stomatal activity, soil depth, rooting effectiveness, and soil moisture content.

6.3.1 Estimating Latent Heat

Remotely sensed surface temperatures can be employed in relationships used to estimate latent heat flux (Jarvis 1981):

$$LE = \rho C_p/\gamma\ (VD_s - VD_a)/R_c \tag{6.6}$$

where ρ = density of the air, C_p = specific heat of air at atmospheric pressure, γ = psychrometric coefficient, VD_s = saturated water vapor density of the air, VD_a = water vapor density of the air, and R_c = stomatal resistance per unit leaf area. In this relationship, it is possible to infer the saturated vapor density, VD_s, for moisture-unlimited surfaces from remotely sensed surface temperature observations, using

$$VD_s = [217/(273.15 + T_s)]\ 6.1078\ e^{((17.269T_s)/(237.0 + T_s))} \tag{6.7}$$

where T_s = observed surface temperature, °C, and the term in brackets transforms Teten's equation for saturation vapor pressure over water to vapor concentration units.

6.3.2 Estimating Sensible Heat

Sensible heat flux can be written

$$H = \rho C_p\ (T_s - T_a)/R_a \tag{6.8}$$

where ρ = density of the air, C_p = specific heat of air at atmospheric pressure, T_a = air temperature above the canopy, T_s = remotely sensed surface temperature, and R_a = the heat transfer resistance between the surface and the air.

Figure 6.1 illustrates a typical late-summer diurnal energy budget for a white pine canopy during a mostly cloud-free day. The variability in fluxes during the afternoon resulted from the influence of clouds. The role of surface temperature in performing the LE and H flux estimations has been described by Eqs. 6.6 and 6.8. Remotely sensed surface temperatures can be determined on a landscape scale. Airborne sensors such as the Thermal Infrared Multispectral Scanner (TIMS) can provide calibrated surface temperature data (Appendix 6.A). The surface temperature measurements can be combined with ground-based measurements of $K\downarrow$, $L\downarrow$, air temperature, water vapor deficits, and estimates of surface resistance to determine the other terms in the equations, and for Eq. 6.4.

6.3.3 Nonradiative Terms in the Thermal Energy Budget

In developing ideas for a primarily remote-sensing means of describing the surface energy budget, we proposed (Luvall and Holbo 1989) a procedure that treated changes in surface temperature as an aggregate response of the dissipative thermal energy fluxes (LE, H, and G) and also expressed the influences of surface properties (canopy structure, amount and condition of biomass, heat capacity, and moisture). We had observed surface temperature changes in data collected by the aircraft-borne TIMS from uniform landscape elements like mature forests, plantations, and clear cuts. These temperature changes were evident when data from successive overflights separated by about 30 minutes were compared. From the

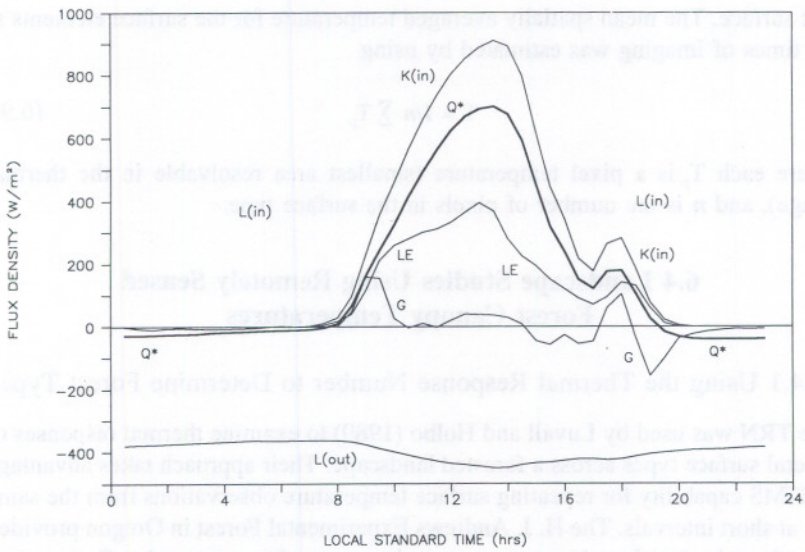

Figure 6.1. Surface energy budget for a white pine plantation at the Coweeta Hydrologic Laboratory, North Carolina. The measurements used to calculate the fluxes were taken with above canopy, tower-mounted, and ground-based instrumentation. The fluxes shown are incoming solar radiation [K↓ = K(in)], incoming long-wave radiation [L↓ = L(in)], net radiation (Q*), latent heat flux, or evapotranspiration (LE), conduction heat exchange (G), and outgoing long-wave radiation [L↑= L(out)]. Cloudiness reduced flux densities during the afternoon.

energy budget, we knew that net radiation, Q^*, constrains the total magnitude of the nonradiative fluxes, and surface-specific Q^* values were used to normalize the measured temperature changes between the different types of surface. Since the rates of the thermal fluxes could be expected to change over the measurement interval, it was reasonable to use the rate of change in surface temperature as the value that reveals how the nonradiative fluxes react to changing radiant energy inputs. We then used the following formulation of the ratio between Q^* and ΔT to define a surface property we called a Thermal Response Number (TRN), which would have units $Jm^{-2}\ °C^{-1}$:

$$TRN = \sum_{t_1}^{t_2} Q^* \Delta t / \Delta T \tag{6.9}$$

where:

$$\sum_{t_1}^{t_2} Q^* \Delta t$$

represents the total amount of net radiation (Q^*) for that surface over the time period between flights ($\Delta t = t_2 - t_1$), and ΔT is the change in mean temperature of

that surface. The mean spatially averaged temperature for the surface elements at the times of imaging was estimated by using

$$T = 1/n \sum T_p \tag{6.9a}$$

where each T_p is a pixel temperature (smallest area resolvable in the thermal image), and n is the number of pixels in the surface type.

6.4 Landscape Studies Using Remotely Sensed Forest Canopy Temperatures

6.4.1 Using the Thermal Response Number to Determine Forest Type

The TRN was used by Luvall and Holbo (1989) to examine thermal responses of several surface types across a forested landscape. Their approach takes advantage of TIMS capability for repeating surface temperature observations from the same site at short intervals. The H. J. Andrews Experimental Forest in Oregon provided a patchwork of various forest types covering a complex topography. Forest types ranged from old-growth Douglas-fir forests to recent clear-cuts.

This study represented the first time that short-term (28-minute) surface thermal response changes have been measured on a "landscape scale" for forests with the use of remote thermal sensors. Each cover type produced a characteristically different TRN (Table 6.1). The sites could be ranked by using the TRN value. The TRN for the forested sites was much greater than for the quarry and clear-cut sites. The TRN even differentiated between similar forested sites. For example, from Table 6.1, it is evident that one could not distinguish between the plantation and the natural regeneration sites by using only surface temperatures. The information shows that it is possible for two different types of forest canopies to have the same temperature, but the TRN indicates the existence of surface properties that result in differences in energy disposition. Thus the TRN, which quantifies the energy required to change surface temperature, also appears to distinguish between various types of surface.

Table 6.1. Surface Rankings Based on Thermal Response Number (TRN) for Douglas Fir Forest Types at the Andrews Experimental Forest, Oregon

Surface Type	Q^* (Wm^{-2})	T (°C)	ΔT (°C)	TRN ($KJm^{-2}\,°C^{-1}$)
Plantation	730	29.5	0.76	1631
Douglas fir forest	830	24.7	0.91	1549
Natural regeneration	771	29.4	1.66	788
Clear-cut	517	51.8	2.16	406
Rock quarry	445	50.7	4.50	168

Forested sites and forest plantations were found to have large TRNs, consistent with their tendency to exhibit moderated microclimates. Clear-cuts and barren sites had quite small TRNs, indicating little capacity to resist microclimate extremes. Sites midway in their development toward becoming forest had intermediate TRN values. The TRN seems to characterize the combined influences of surface properties controlling microclimate processes.

6.4.2 Using Remotely Sensed Surface Temperatures to Estimate Evapotranspiration

A few studies have used remotely sensed data from aircraft-borne scanners for estimating forest ET (Luvall 1988; Pierce and Congalton 1988). Luvall (1988) directly compared ET rates determined with the use of remotely sensed surface temperature from the TIMS with tower-based measurements of ET determined by using the energy budget approach (Penman-Monteith; Monteith 1973) from a white pine canopy. The initial results indicated a close agreement between the Penman-Monteith estimates and the TIMS (Table 6.2).

6.4.3 Spatial Heterogeneity of Forest Canopy Temperature

The spatial variation of canopy temperatures across the landscape produces a complex pattern. Differential solar loading due to topography can produce significant spatial variation of canopy temperatures even in monospecific canopies of uniform age and structure (Fig. 6.2). The white pine canopy temperatures ranged from 14.2°C to 18.8°C within the 14.1-ha south-facing watershed.

Observations made simultaneously across a landscape with the use of TIMS show that different surface types take on a wide range of temperatures with different surface temperature frequency distribution patterns (Fig. 6.3, from Holbo and Luvall 1989). Each type of surface appears to have uniquely influenced its pattern, apparently the result of its thermal properties and microclimates.

The distributions were strongly controlled by the presence of a plant canopy: distributions are markedly broader and warmer where a plant canopy is absent

Table 6.2. Evapotranspiration Estimated for a White Pine Canopy Using TIMS-Derived Surface Temperatures and the Penman-Monteith Equation

	Time Ending					
Latent energy flux (Wm^{-2}) (Evapotranspiration)	8:25 a.m.	8:55 a.m.	1:00 p.m.	1:25 p.m.	7:30[a] p.m.	8:00[a] p.m.
Penman-Monteith method	44	308	387	422	—	—
TIMS-based method	55	395	450	492	—	—

[a] Stomata were closed.

Figure 6.2. A thermal image composed of 5-m resolution TIMS temperature data acquired from a morning flight (8:30 a.m.) of the 28-year-old white pine plantation at Coweeta, for which the energy budget is shown in Fig. 6.1. Notice the variability in canopy temperatures within the watershed, shown by differences in shading, even though the canopy is of uniform age and structure. The variability was apparently the result of differences in incoming solar radiation because of differences in topographic position.

[e.g., the clear-cut (Fig. 6.3d)] and sensitive to the spatial uniformity of canopy elements on the site [e.g., the narrow distribution of the mature Douglas-fir stand (Fig. 6.3a) versus the broader distribution of the naturally regenerating, more sparsely occupied site (Fig. 6.3b)]. At night, although the range in temperatures is smaller, the thermal image still seems to capture subtle variations that may be as characteristic of surface type as during the daytime. In both day and night situations, the thermal images appear to have potential for helping to increase understanding of the dominant physical processes operating at the surface.

Areas of incomplete canopy coverage, as well as clear-cut areas, often exhibit extreme differences between needle temperatures and soil surface temperature. Vanderwaal and Holbo (1984) showed that Douglas-fir needle temperatures tracked air temperatures very closely (±3°C). However, sunlit soil surface temperatures directly under the seedlings were 30°C to 50°C higher than either air or needle temperatures. In such cases, one could not use an average surface temperature for the estimation of LE or H from the forest canopy without substantial errors.

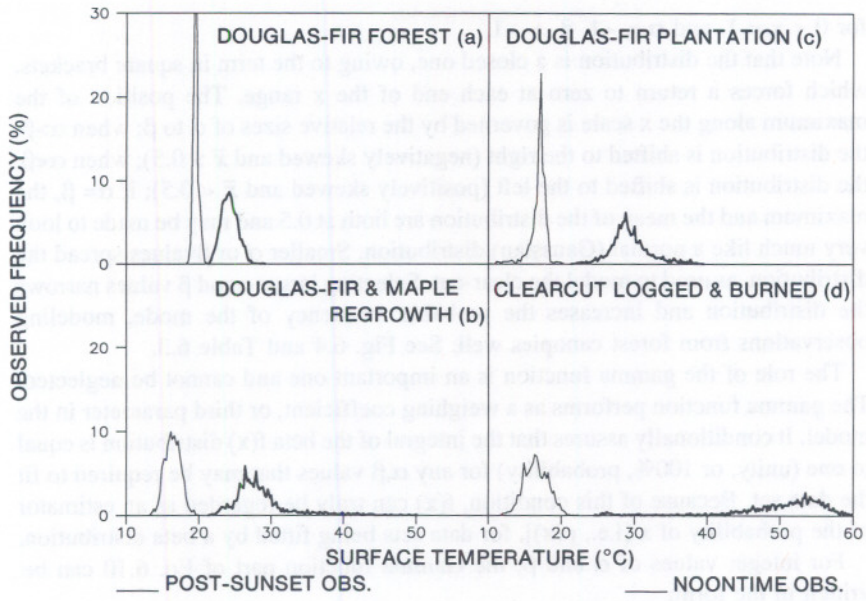

Figure 6.3. TIMS surface temperature frequency distribution patterns for four landscape types at the H. J. Andrews Experimental Forest in the Oregon Cascade Mountains: (a) a Douglas-fir forest; (b) a naturally regenerating site with an incomplete canopy coverage of about 60% Douglas fir and 40% maple; (c) a fifteen-year-old Douglas fir plantation; and (d) a clear-cut, logged and burned two years earlier. The two sets of data values for each type of surface represent night (lighter line) and day (heavier line) temperature distributions respectively.

Therefore, the average surface temperature observations may not characterize all the spatial variability needed for energy budget flux estimates. However, as demonstrated by Holbo and Luvall (1989), the frequency distributions of temperatures can be used as a powerful model in the differentiation and identification of land surface cover types and their properties. They found that a beta probability distribution can be closely fitted to surface temperature frequency distributions for a wide variety of forest landscapes. One advantage of using the beta distribution as a model is that it utilizes the pixel frequency distributions directly, and no high-order, measurement-error-magnifying statistics are used. (There is always a quantizing error in digital data that will propagate exponentially into the higher statistical moments.)

A beta probability distribution can be fitted to any closed distribution assumed to have a single mode (Selby 1968; Press et al. 1986). It is defined by two parameters (α, β) and a gamma (Γ) function of these same two parameters:

$$f(\mathbf{x}) = \Gamma(\alpha,\beta)[\mathbf{x}^{\alpha}\ (1 - \mathbf{x})^{\beta}] \tag{6.10}$$

for $0 < x < 1$, and $\alpha > -1$, $\beta > -1$.

Note that the distribution is a closed one, owing to the term in square brackets, which forces a return to zero at each end of the x range. The position of the maximum along the x scale is governed by the relative sizes of α to β; when $\alpha>\beta$, the distribution is shifted to the right (negatively skewed and $\bar{x} > 0.5$); when $\alpha<\beta$, the distribution is shifted to the left (positively skewed and $\bar{x} < 0.5$); if $\alpha= \beta$, the maximum and the mean of the distribution are both at 0.5 and may be made to look very much like a normal (Gaussian) distribution. Smaller α or βvalues spread the distribution, as used to model the clear-cut. Selecting larger $\alpha$and β values narrows the distribution and increases the probable frequency of the mode, modeling observations from forest canopies well. See Fig. 6.4 and Table 6.3.

The role of the gamma function is an important one and cannot be neglected. The gamma function performs as a weighing coefficient, or third parameter in the model. It conditionally assures that the integral of the beta $f(\mathbf{x})$ distribution is equal to one (unity, or 100%, probability) for any α,β values that may be required to fit the data set. Because of this condition, $f(\mathbf{x})$ can truly be regarded as an estimator of the probability of $\mathbf{x}$ [i.e., $p(\mathbf{x})$], for data sets being fitted by a beta distribution.

For integer values of α and β, the Gamma function part of Eq. 6.10 can be written in the form:

$$\Gamma(\alpha,\beta) = [\Gamma(\alpha + \beta + 2)]/[\Gamma(\alpha + 1)\Gamma(\beta + 1)] \tag{6.11}$$

defining $\Gamma(\mathbf{y}) = (\mathbf{y} - 1)!$, where ! is the factorial operation, and $\mathbf{y}$ is the sum of values in parentheses. A description of the computational technique for determining parameters α and β is presented in Appendix 6.B.

Beta modeling has the potential to become a useful tool for describing, comparing, and classifying thermal image data sets; see Table 6.3 (from Holbo and Luvall 1989). In the table, α and β beta parameters for several forest types at the H. J. Andrews Experimental Forest are shown. With the model parameters, the surface temperature distributions can be compared. The α and β values vary widely and can be seen to relate strongly to surface type. An index, the beta index, has been devised to simplify the comparison. The index is a consolidation of the beta model's parameters into a single number that conveys the same information, although a bit of contrast stretching has been introduced (see Appendix 6.B).

6.4.4 Forest Edge Microclimates

Figure 6.5 shows two surface temperature profiles, one at noon and one after sunset, taken along a transect trending from southwest to northeast through a clear-cut on the H. J. Andrews forest (Fig. 6.6). Each profile shows the same ground, differing only in the time of imaging. The transect begins in the forest at the edge of the clear-cut, then moves across its logged and burned southwest slope,

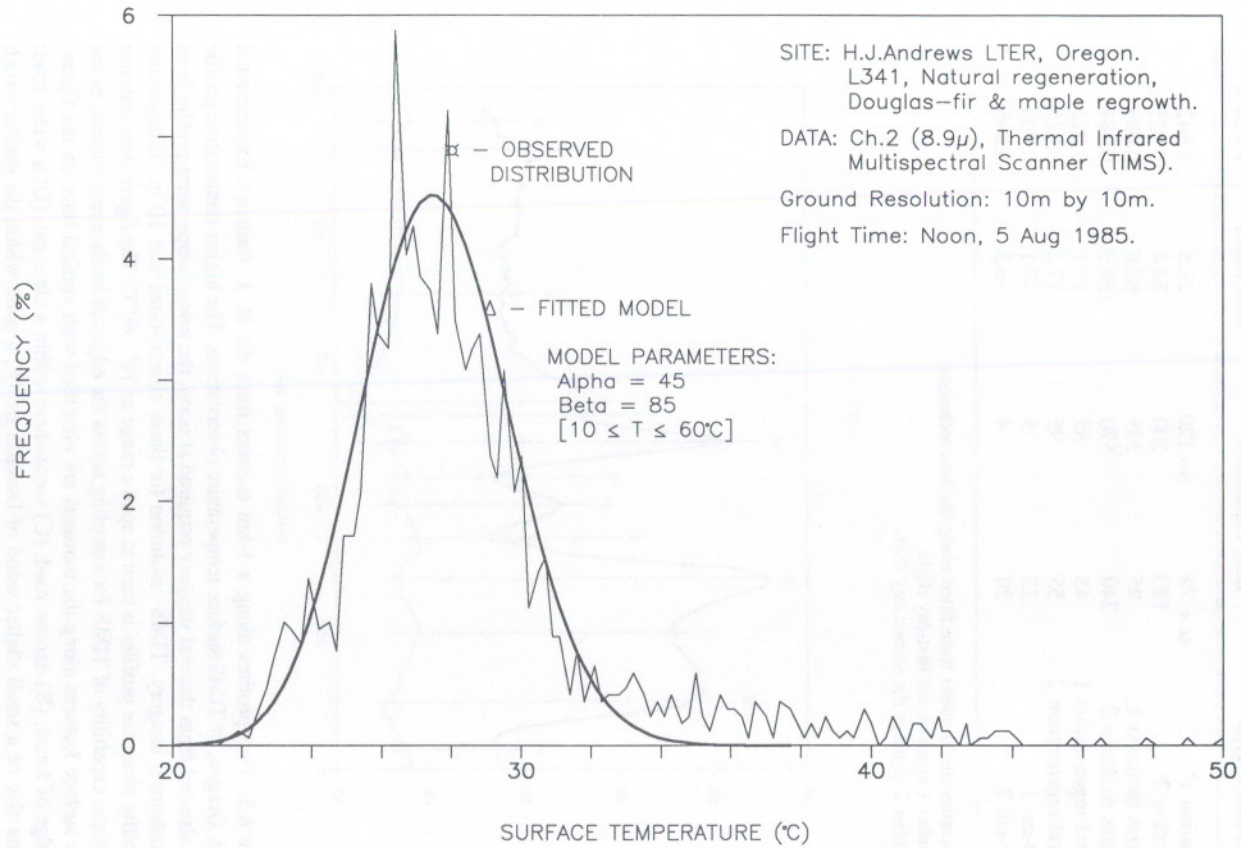

Figure 6.4. An example of an observed surface temperature frequency distribution (irregular line) and its modeled beta distribution fit (smooth, heavier line). This example is of the H. J. Andrews natural regeneration surface type from first overflight of TIMS. The beta parameters producing the fitted curve are $\alpha = 45$ and $\beta = 85$. The major features of the surface temperature frequency distribution are well described by the beta probability distribution.

Table 6.3. Comparisons of Four Surface Temperature Distributions from the H. J. Andrews Experimental Forest, Oregon[a]

Surface Type	Beta Parameters		Beta Index	Fitted R^2
Plantation 1[b]	$\alpha = 70$	$\beta = 120$	21.5	0.942
Plantation 2[c]	120	200	34.4	0.925
Douglas fir forest 1	95	245	62.8	0.989
Douglas fir forest 2	240	570	138.9	0.984
Natural regeneration 1	45	85	17.1	0.923
Natural regeneration 2	55	95	17.2	0.925
Clear-cut 1	23	5	−7.1	0.900
Clear-cut 2	20	4	−6.3	0.896

[a] Frequency distributions were fitted using the beta technique.
[b] Number 1 signifies the first-day flight.
[c] Number 2 signifies the second-day flight.

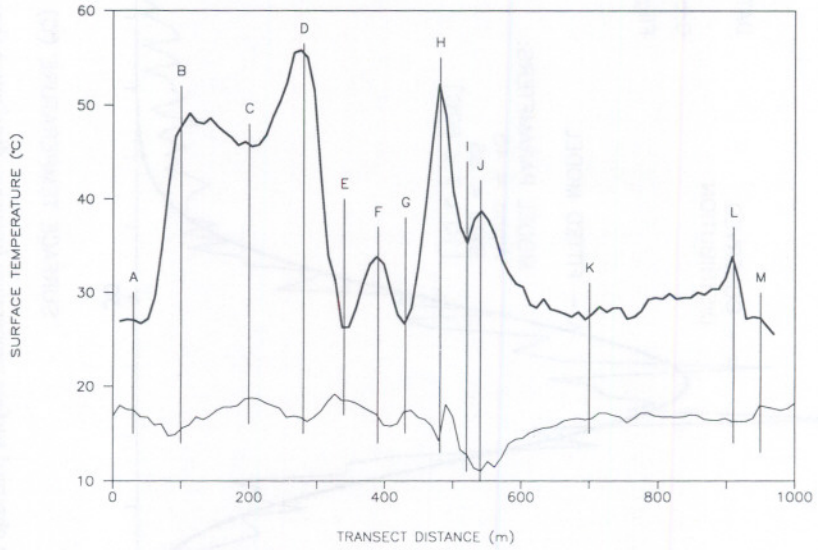

Figure 6.5. Two profiles along a 1-km transect from the H. J. Andrews Experimental Forest, Oregon, of TIMS surface temperature observations. The higher temperature profile was extracted from thermal imagery acquired at noon, the lower temperature profile from the postsunset imagery. TIMS resolution for these observations was 10 m. Temperature variability along the profiles is seen to span a range of 10°– 60°C. The figure demonstrates the unique capability of TIMS for sampling across the edges of landscape elements. Some of the surface features along the transects are identified with vertical lines on the figure: (A) edge of forest; (B) narrow road; (C) somewhere within a clear-cut; (D) a wider road; (E) one side of a small shelter wood of Douglas fir; (F) a pond within the shelter wood; (G) the other side of the shelter wood; (H) the wide road; (I) trees along road; (J) in a flatter part of the clear-cut; (K) somewhere within a 15-year-old Douglas fir plantation; (L) a trail; and (M) in an older stand of Douglas fir regrowth.

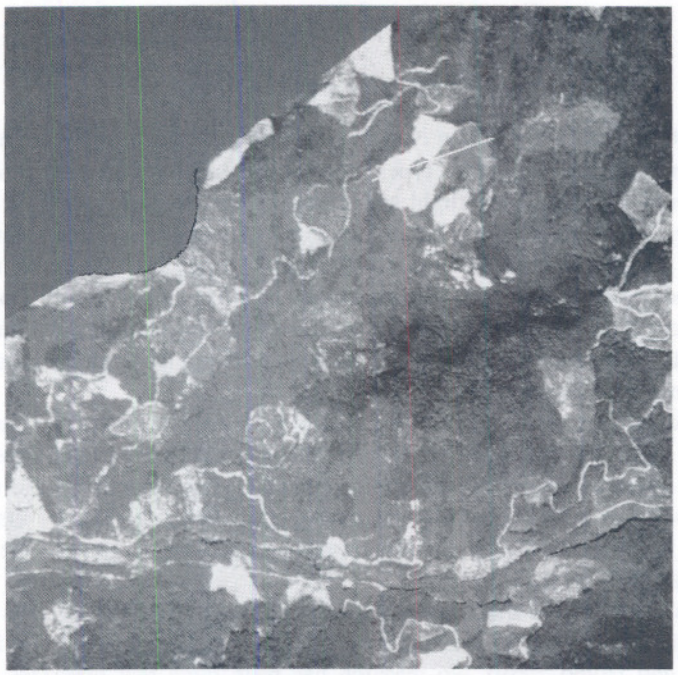

Figure 6.6. One of the TIMS images used to obtain the temperature transect data for Fig. 6.5. The white line, from lower left (SW corner) to upper right (NE corner), shows the direction of the transects.

through an isolated stand of mature Douglas fir, across a flatter part of the same clear-cut, and across a fifteen-year-old Douglas fir plantation.

From the profiles, it appears that surface temperature transitions across the known abrupt boundaries, as between forest and clear-cut, are about 30 m in length. But it must be appreciated that each observation point along the transect represents the average temperature of a 10 m by 10 m surface area (the pixel size for this data set), thus limiting edge definition to lengths longer than twice the width of a pixel in the direction of the transect. Nevertheless, it would be difficult to improve upon this with ground-based sampling.

A meteorological station on the same clear-cut (near D in Fig. 6.5) measured average air temperatures (at 2-m height) of 25°C during the noon imaging overflight and 14°C during the evening imaging. However, all points along the transect were warmer than the noontime air temperature, with a few exceeding 55°C. Just after sunset, most points were slightly warmer than the air, with a small section along the transect (J) dropping to nearly 10°C. This region, near (J), seems to indicate the onset of cold air drainage from upslope, apparently being impeded by something in that part of the clear-cut.

6.5 Limitations of Thermal Techniques

6.5.1 Thermal Response Number

Some site-specific information is needed for calculation of the TRN for optimal discrimination of forest canopy types. Specifically, one must know incoming solar radiation at the time of the flight and determine the net radiation for a range of forest types. The relationship between $K\downarrow$ and Q^* is well established, and generally the literature values can be used (Oke 1987). Sites at which $K\downarrow$ is routinely measured are relatively rare. (Its measurement is prescribed for all Long-Term Ecological Research sites.) Also, Q^* can be calculated by using Eq. 6.5. Luvall and Holbo (1989) showed that errors in Q^* estimates would not significantly affect the TRN ranking of forest types.

At the present time the TRN technique is limited to aircraft-obtained data. Aircraft and calibrated thermal sensors are limited in number and expensive to operate. Weather conditions ideal for obtaining the measurements are rigorous. Data from sites with frequent cloud cover (e.g., tropical forests) are limited and difficult to obtain. In rapidly changing weather conditions, it may also be difficult to obtain repeated aircraft passes.

The use of TRN to describe landscape functional processes is in its infancy. Only a limited number of sites for western coniferous forest have been described (Luvall and Holbo 1989). No research has been done that describes seasonal variability in the TRN. TIMS data has been collected by the authors during 1987 and 1988 from several tropical and eastern deciduous forests. Preliminary analysis of that data supports the use of the TRN for landscape function analysis in those ecosystems.

6.5.2 Estimating Evapotranspiration

The determination of LE with remotely sensed surface temperatures through the use of Eq. 6.6 requires that several plant or surface-dependent variables be known. First, measured or good models of the canopy conductances are needed to account for the plant physiological control of water loss. This information may not be readily available for the forest or during the time frame of the flights.

Canopy conductance is one of the most difficult factors to estimate accurately. Plant species have different rates of transpiration and stomatal conductance, both daily and seasonally. In forested ecosystems, evergreen, coniferous tree species tend to have lower rates of transpiration and stomatal conductance than deciduous, broad-leaved species. A wide variation in transpiration and conductance has been reported among species. Since ET is directly related to canopy conductance, it can differ between forests or stands because of species composition, as well as the environment (Chambers et al. 1985; Federer and Gee 1976; Hinckley et al. 1981).

Second, it is difficult to determine the vapor pressure gradient to which the forest canopy is actually exposed. Usually, vapor pressure information is measured at one site within the study area and taken as representative of the area.

Since most remotely sensed data is taken at a instantaneous point in time, the measurements must be extrapolated for the whole day. Several approaches have been taken to equate the two ET estimates. Nieuwenhuis et al. (1985) proposed the following relationships in terms of surface temperature and latent heat flux (following the notation and formulations used by Gash 1987):

$$LE_d = LE_{ref.d} - B^1(\delta T_s)_i \quad (6.12)$$

where LE = latent heat flux (evapotranspiration), d = the 24-h average values, ref = reference evapotranspiration, i = to an instantaneous midday value, B^1 = a calibration constant similar to the constant B proposed by Jackson et al. (1977), which related the difference between surface and air temperature to evaporation, and δT_s = surface temperature.

6.5.3 Surface Temperature Distributions

The information content of any distribution function is constrained by the size and number of the samples taken and is always limited by practical considerations. For the surface temperature distributions modeled here by beta probability distributions, it was fortunate that pixel sizes were 10 by 10 m. This size is near the upper limit of what could be reasonably expected to be descriptive in a forested landscape, since the dominant surface features (crowns of the trees and shrubs) frequently approximately that size. Should a subsequent examination of the same surface types on the same landscape be performed with the TIMS flown at lower altitudes to achieve a resolution of 5 by 5 m, better surface-type discrimination would be expected. And, if flown at a coarser resolution, say 20- by 20-m pixels, details would be lost to the extent that recognition of only the most dramatically different landscape elements would be obtained. As a rule, the information content of a collection of samples is strictly interpretable only to those elements in the sample space which are twice as large as the spatial resolution of the sampling process. This rule is analogous to Shannon's sampling theorem (1949), which was developed for extracting information from temporal phenomena. This is not to conclude that the smaller elements exert no influence on the individual samples, but rather to caution against attempting to extract significance from the data at scales smaller than the sampling can support.

Another factor limiting the broader applicability of beta distribution modeling to landscape elements of differing types is that only a few TIMS missions have been flown for the purpose of collecting thermal images of other landscape types. The majority of the flights have been flown to exploit the potential of TIMS to acquire imagery for interpreting surface geology across desert landscapes.

It is certainly anticipated that temporal variability, caused by changing solar angles or redistribution of components of the energy budget, will influence the distributions of surface temperatures. One example might be a water-stressed canopy, where the partitioning of Q^* shifts from LE to H as stomata close late in the day. In this instance, canopy temperatures might be expected to increase, in

response to the need to dissipate a greater proportion of the energy as sensible heat. While the potential impact of such effects should not be ignored, the analyses conducted thus far suggest that beta modeling will detect contrasts between different landscape elements during fair weather. Part of this success may be attributable to the fact that the energy budgets of different surface types respond to the conditions at any given time in ways that are consistent with, and characteristic of, their specific surface type.

6.6 Uses of Thermal Models in Landscape Ecology

Surface temperature is of importance to many ecological processes. Together with moisture availability, surface temperature can encourage or restrict the initiation of plant life on a site. Until the advent of spatial surface temperature sampling by instruments like TIMS, management of the microclimate of plant establishment depended largely upon relationships based on air temperature measurements. However, air temperature is far more conservatively behaved and rarely reveals the true extremes experienced by plants (and animals) at the surface. There are several areas in which thermal models can be used in landscape ecology.

6.6.1 Plantation Forestry

Plantation forestry is one area where avoidance of surface temperature extremes is critically important to the success of reforestation efforts (Childs et al. 1985). The experienced manager may have intuitive beliefs about this type of environment. However, a site-specific investigation, as exemplified in Fig. 6.5, can improve the manager's objectivity with regard to the actual conditions at the surface.

6.6.2 Evaluation of Thermal Habitats of Fish and Wildlife

Increasing utilization of the landscape has resulted in greater competition for resource values in some areas. For example, as logging activities encroach upon the boundaries of small mountain streams, it is critical to ensure adequate shading to prevent water temperatures from rising to uninhabitable levels for desired fish species. Thermal imagery could be used to gauge the effectiveness of buffer strips along riparian zones or to help locate stretches that might need special protective measures.

6.6.3 Frost Protection Planning for Nurseries and Orchards

Thermal images can reveal the presence of cold air collection areas and drainage paths when a foliar cover is present. High-elevation grasslands and clear-cuts become sources of cold air. Forests exhibit much smaller changes in temperature from day to night. Forest canopies may extend into warmer air aloft, in effect buffering the intrusion into the canopy space of colder surface air (Holbo 1983). Nighttime radiation losses of nonforested surfaces under cloud-free skies are about

50 Wm^{-2} (Holbo and Childs 1987). Since $L\uparrow = \varepsilon\sigma T^4$, one can use its derivative, $\delta L\uparrow/\delta T = 4\varepsilon\sigma T^3 \cong 5\ Wm^{-2}°C^{-1}$, to estimate that each 1°C drop in surface temperature represents an additional 5 Wm^{-2} differential in the radiation balance, progressively accelerating the heat loss rate and increasing the chance of freezing.

6.6.4 Predicting Nighttime Air-Shed Smoke Impact

The cold air drainage patterns also identify areas that tend to entrain smoke originating with controlled burning activities, such as slash burning done following logging and field burning of grass stubble following seed harvesting. These activities are subject to increasing regulation, especially near population centers. Studies of thermal imagery before scheduling a burn might help managers avoid violations of regulations and could be used for mapping areas likely to provide routes for nighttime air drainage (Gossmann 1986).

6.6.5 Estimating Evapotranspiration

Water is a critical resource. Although concern for its conservation has waned, there will be a renewal of interest in improved evapotranspiration estimation techniques if current trends continue. A substantial amount of effort has already been expended on the development of evapotranspiration estimation methods that use remotely sensed thermal data as a primary input variable (e.g., Abdellaoui et al. 1986; Heilman et al. 1976; Ho 1985; Reginato et al. 1985; Seguin and Itier 1983; Soer 1980; Stone and Horton 1974). With the improved spatial resolution and surface temperature accuracy offered by the TIMS, those methods can now be made site specific and have greater relevance to landscape management practices (Luvall 1988).

6.6.6 Detection and Delineation of Microtopographic Terrain Features

The direct linkage between thermal emissions from a surface and its physical properties (e.g., thermal diffusivity) permits the extraction of information about features too subtle to appear in unenhanced thermal images (Pelletier 1985; Pelletier et al. 1985). Features that can be located in this way include soil conservation measures, minor drainages, and archaeological structures.

6.6.7 Assessment of Vegetatively Moderated Urban Microclimates

Microclimatic issues are important to urban planners. Structural materials within the urban environment often result in hostile microclimates. By using remotely sensed thermal image data, the influence of various amounts and arrangements of vegetation in those environments can be evaluated and mediating alternatives recommended (Quattrochi and Rowntree 1988).

6.6.8 Recognition of Landscape Type with Thermal Image Data

Thermal remote sensing offers many possibilities for studying landscapes because there is virtually no other means by which the spatial character of the surface

temperature field in those systems can be observed. This spatial character tends to be diagnostic of the type of surface from which the thermal image is taken. For example, Fig. 6.3 contains observed (nighttime and daytime) frequency distributions of surface temperature of four landscape types. It can be seen that each surface type exhibits a different pattern of dispersion, which is especially obvious in the daytime.

By using a beta probability distribution as a model, these patterns can be described in terms of just two parameters (Holbo and Luvall 1988). Different landscape types yield unique combinations of these parameters. It should be feasible to implement this technique for landscape recognition. Furthermore, because of the microclimatic information also available from this data, its association with specific landscape types should improve regional evapotranspiration estimation methods.

6.6.9 Predicting Microclimatic Change Due to Landscape Type Conversion

The interrelationships among the four components of a surface's thermal energy budget (radiation, convection, conduction, and latent heat (i.e., evapotranspiration) make it difficult to predict the consequences of converting from one landscape type to another. These components respond to both external and internal factors, but it is the internal biophysical properties of the site that are changed by management practices. When complicated even more by multiple land management practices across a landscape, assessing the net impact is beyond the scope of traditional approaches. A new approach, arising out of the study of short-term changes in surface temperature and made with the use of TIMS, has been proposed. It is based on a derived surface property called the TRN (Luvall and Holbo 1989).

6.7 Summary

Thermal remote sensing offers special and unique qualities to the landscape ecologist that cannot be obtained from other kinds of remote sensing data products. Thermal remote sensing instruments measure a very fundamental surface phenomenon, namely, temperature, a primary expression of the physical environment. Because temperature data can be used to evaluate functional relationships, such as the energy budget, thermal remote sensing can become a valuable tool for improving our understanding of patterns and processes in landscape ecology. This is especially true for instruments like the TIMS, which offer measurement accuracy and spatial resolution far better than previously attainable.

Immediate applications for remotely sensed thermal imagery and the corresponding temperature data include avoiding or managing stressful microclimates (high temperature/low moisture) in plantation silviculture or cropland agriculture; frost protection planning for nurseries and orchards; watershed, crop, or forest evapotranspiration estimation; evaluation of thermal habitats of fish and wildlife

(buffer strip effectiveness along mountain streams or in riparian zones); predicting nighttime air-shed smoke impact regions during controlled burns; thermal recognition and classification of landscape types; predicting microclimatic change due to landscape type conversion (fire, logging); detection and delineation of microtopographic terrain features (soil erosion control structures, locating archaeological sites); and assessment of vegetatively moderated urban heat islands.

The analytical models and image processing techniques that have been presented here are in their initial stages of development. The applications examples posed are just a few of those which come to mind when we consider the large potential for landscape applications that this remote sensing technology appears to have. Improvements are already being planned for the instrumentation, so that the next generation of TIMS will have better spatial resolution and measurement precision. Work is also under way to make thermal data processing easier, with more of the image-handling tasks being transferred to microcomputers and thus becoming accessible to more researchers.

Appendix 6.A: Obtaining Calibrated Remotely Sensed Canopy Temperatures

The Thermal Infrared Multispectral Scanner (TIMS) is an aircraft-mounted instrument (Palluconi and Meeks 1985). It was used to obtain the surface temperature measurements needed for investigating forest canopy thermal response and for the development of an analytical model of surface temperature distributions. The TIMS has six channels in the thermal wavelength region from 8.2 to 12.2 μm (Fig. 6.7). It scans a swath 60° wide along the flightline to capture images of the surface in raster style. The TIMS is continuously calibrated through the use of on-board reference blackbody cavities, which results in a noise equivalent temperature (NEΔT) as low as 0.09°C for channel 2 and a precision of 0.2°C over the temperature range of 10 to 65°C. Its spectral responsivity and blackbody radiance calibration coefficients are determined from preflight optical bench calibrations. The on-board low and high temperature blackbodies are read at the beginning and end of each raster's scan line. The blackbody temperatures are selected to bracket the expected range of surface temperatures to optimize TIMS' temperature resolution. Spatial resolution can be varied from 5 to 30 m, depending on aircraft altitude.

It is necessary to account for atmospheric radiance to obtain accurate surface temperature data. Although TIMS' channels fall within the so-called atmospheric window for long-wave transmittance (8.0 to 13.0μm), the maximum transmitance there is actually only about 80%, meaning that some 20% of the radiance received by TIMS' thermal sensing element may originate in the path between the surface to the sensor. Ground-based measurements show that the incoming (down-welling) long-wave energy flux density ($L\downarrow$) from the atmosphere varies from 300 to 425 Wm^{-2}, of which some 60 to 85 Wm^{-2} might be interpreted as caused by long-wave emission from the surface. Atmospheric radiance is mostly a function of the amount and temperature of water vapor.

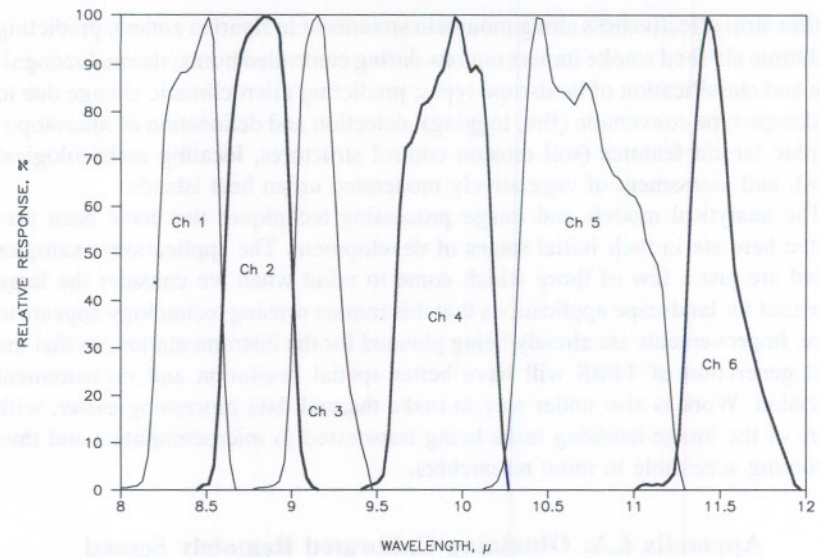

Figure 6.7. The spectral response curves for the six channels of TIMS. Channel 2 appeared to offer the best accuracy and was used to obtain surface temperature data presented here.

Atmospheric radiance can be determined in one of two ways: (1) measuring $L\downarrow$ by using an pyrgeometer (typical passband of 5 to 50 μ), which then is adjusted according to the specific wavelengths used by TIMS (Sweat and Carroll 1983); or (2) measuring the atmospheric profiles of air temperature and water vapor content and then estimating the amount of radiance correlation from these measurements. At many meteorological stations throughout the United States, such profiles are routinely taken using radiosondes twice daily (commonly at 6:00 a.m. and 12:00 midnight). The authors used the second approach, but employed on-site, TIMS flight-time concurrent radiosonde launches to obtain the profile data. The atmospheric profiles were then incorporated in the LOWTRAN6 model for calculation of atmospheric radiance (Kneizys et al. 1983). Atmospheric long-wave radiance values calculated by an earlier version, LOWTRAN5, have been shown to be in excellent agreement with measured atmospheric radiance values (Sweat and Carroll 1983). Wilson and Anderson (1986) endorsed the validity of LOWTRAN5 for atmospheric radiance corrections of aircraft thermal data collected over atmospheric path lengths similar to those used here.

The output from LOWTRAN6 is then combined with TIMS' spectral response curves, using the module TRADE on the ELAS system at NASA's Stennis Space Center, Science and Technology Laboratory (Graham et al. 1986). TRADE produces a look-up table for pixel temperatures as a function of TIMS values (Anderson 1985).

Appendix 6.B: Modeling Observations with a Beta Probability Distribution

A TIMS data set can be modeled with a beta probability distribution. The following describes the steps used:

1. Scale the TIMS temperature values from the observed frequency distribution data set to range from 0 to 1:

$$\mathbf{x} = (T_j - T_{low})/(T_{high}) - T_{low})$$

where low and high are the extreme TIMS temperature values, and

$$T_{low} \leq T_j \leq T_{high}$$

2. Choose values for α and β and compute for each $\mathbf{x}$:

$$\mathbf{x}^{\alpha}(1 - \mathbf{x})^{\beta}$$

Near 0 and 1 of $\mathbf{x}$, this beta product function will produce very small numeric values, so small that computational difficulties may be experienced. Such situations arise when a frequency distribution is narrow and has large frequency classes, thus requiring large values of α and β.

3. Compute the integral function of the values obtained by step 2 for successive $\mathbf{x}_i$ over the interval $0 \leq \mathbf{x} \leq 1$:

$$f(\mathbf{x}_i) = \int_0^{x_i} \mathbf{x}^{\alpha}(1 - \mathbf{x})^{\beta}\, \delta\, \mathbf{x}$$

If the data intervals are equivalent for all data sets, this may be done by successively summing the results of step 2 for $\mathbf{x}_i$ over its 0 to 1 range.

4. Normalize the function described by step 3 according to its value at $\mathbf{x} = 1$. In step 3, this maximum value will likely be a small number. Dividing it into all values of the function produced in step 3 will result in a function produced by this step (step 4), which is a cumulative beta distribution with an integral value of unity at $\mathbf{x} = 1$. This step performs an equivalent operation to the coefficient $\Gamma(\alpha, \beta)$, which is otherwise troublesome to compute.
5. Differentiate the resultant function of step 4 at the intervals of $\mathbf{x}$. This produces the beta probability density function (PDF) of α, β, or $p(\mathbf{x})$.
6. Compare $p(\mathbf{x})$ with the observed frequency distribution. Loop iteratively from step 2 (selecting new trial values of α and β) through step 6 until an acceptable level of comparability is found. For the cases shown here, a combination of least squares fit and visual (graphical) matching at the modal frequency was used. This combination approach helped avoid choosing an α, β parameter set that may yield a high regression coefficient but that does not simultaneously represent the modal class of the observed distribution.

The regression test was made a part of the fitting procedure. The fitting procedure utilized only those frequencies within the TIMS-observed pixel temperature range, excluding the tails of the beta distribution, which were beyond the low-high range of the data set. By using the regression, a succession of α and β values were tried until a maximum R^2 was found. Tabulating the resulting R-squared values in the form of an $[\alpha,\beta]$ matrix helped in the process of choosing the best parameter combination. With the use of such a matrix table, the optimal α and β values were chosen from along what appears as a diagonal "ridge" of higher correlation coefficients. This iterative technique was also assisted by viewing graphs of the "fit" on a graphics monitor, since the convergence of α and β values toward an optimum could be visually evaluated, especially during the early stages of fitting. Additionally, viewing the fit helped ensure against selecting α and β values that may happen to yield a high R^2 but fail to satisfactorily produce the frequency near the principal mode of the distribution. This was often the situation for the more irregular data sets. Also, in view of the wide range in α and β combinations representing all observed surface temperature distributions in the Andrews data sets, the regression-fitting technique seemed to provide fairly adequate discrimination among the sites examined.

To make ranked comparisons between sites, the two beta parameters can be combined into a single value, or beta index. This index contains information about both the parameter ratio and parameter magnitudes. The fitted α, β values for the sites had absolute ratios of less than 1 to above 3, at the same time ranging over three orders of magnitude: $1 < \alpha/\beta$ (or β/α) < 1000, or more. The geometric mean (GM) of α, β, $\sqrt{\alpha\beta}$ was selected to represent magnitude information. The logarithm of the β/α ratio (LR), $\log_{10}(\beta/\alpha)$, was chosen to convey the relationship between α and β. The advantage of this logarithmic form is twofold: first, it indicates model asymmetry in a manner similar to the third moment of the data set, the second, it offers greater discrimination between distributions having ratios close to unity, essentially stretching the contrast level for scenes with narrow and/or nearly symmetrical temperature frequency distributions, i.e., the nighttime data sets. The beta index was formed as the product of these two terms: GM times LR.

References

Abdellaoui, A.; Becker, F.; and Olory-Hechinger, E. 1986. Use of Meteosat for mapping thermal inertia and evapotranspiration over a limited region of Mali. *Journal of Climate Applied Meteorology* 25:1489–1506.

Anderson, J.E. 1985 Thermal infrared data: its characteristics and use. American Society for Photogrammetry and Remote Sensing Technical Paper 1:143–55.

Chambers, J.L.; Hinckley, T.M.; Cox, G.S.; Metcalf, C.L.; and Aslin, R.C. 1985. Boundary-line analysis and models of leaf conductance for four oak-hickory forest species. *Forest Science* 31:437–50.

Childs, S.W.; Holbo, H.R.; and Miller, E.L. 1985. Shadecard and shelterwood modification of the soil temperature environment. *Soil Science Society of America Journal* 49:1018–22.

Federer, C.A., and Gee, G.W. 1976. Diffusion resistance and xylem potential in stressed and unstressed northern hardwood trees. *Ecology* 57:975–84.

Garnier, B.J., and Ohmura, A. 1968. A method of calculating the direct shortwave radiation income of slopes. *Journal of Applied Meteorology* 7:796–800.

Gash, J.H.C. 1987. An analytical framework for extrapolating evaporation measurements by remote sensing surface temperature. *Internation Journal of Remote Sensing 8:1245–49.*

Gossman, H. 1986. The influence of geography on local environment as inferred from night thermal infrared imagery. *Remote Sensing Review* 1:249–75.

Graham, M.H.; Junkin, B.G.; Kalcic, M.T.; Pearson, R.W.; and Seyfarth, B.R. 1986. ELAS-Earth Resources Laboratory Applications Software, rev. January 1986. NASA/NSTL/ERL Report Number 183.

Heilman, J.L.; Kanemasu, E.T.; Rosenberg, N.J.; and Blad, B.L. 1976. Thermal scanner measurement of canopy temperatures to estimate evapotransportation. *Remote Sensing of Environment* 5:137–45.

Hinckley, T.M.; Teskey, R.O.; Duhme, F.; and Richter, H. 1981. Temperate hardwood forests. In *Water Deficits and Plant Growth,* vol. 6,pp. 153–208. New York: Academic Press.

Ho, D. 1985. Soil thermal inertia and sensible and latent heat fluxes by remote sensing. In *Proc. 4th Thematic Conference: Remote Sensing for Exploration Geology,* pp. 635–43. San Francisco, April 1–4, 1985. Ann Arbor: Environmental Research Institute of Michigan.

Holbo, H.R. 1983. Wind Patterns in a clearcut and an adjacent forest. FIR Report 5(2). Oregon State University Cooperative Extension Service.

Holbo, H.R., and Childs, S.W. 1978. Summertime radiation balances of clearcut and shelterwood slopes in southwest Oregon. *Forest Science* 33:504–16.

Holbo, H.R., and Luvall, J.C. 1988. Thermal responses and surface temperature distributions of forested landscapes. In *Remote Sensing for Resource Inventory, Planning and Monitoring*, ed. J.D. Greer, pp. 308–17. Falls Church, Va.: American Society for Photogrammetry and Remote Sensing.

Holbo, H.R., and Luvall, J.C. 1989. Modeling surface temperature distributions in forest landscapes. *Remote Sensing of Environment* 27:11–24.

Jackson, R.D.; Reginato, R.J.; and Idso, S.B. 1977. Wheat canopy temperatures: a practical tool for evaluating water requirements. *Water Resources Research* 13:651–56.

Jarvis, P.G. 1981. Stomatal conductance, gaseous exchange and transpiration. In *Plants and Their Atmospheric Environment*, eds. J. Grace, E.D. Ford, and P.G. Jarvis, pp. 175–204. Oxford: Blackwell.

Kneizys, F.X.; Settle, E.P.; Gallery, W.O.; Chetwynd, J.H., Jr.; Abreu, L.W.; Selby, J.E.A.; Fenn, R.W.; and McClatchey, R.A. 1983. Atmospheric transmittance/radiance: computer code Lowtran-6. Air Force Geophysics Laboratory Report AFGL–TR83–0187. Optical Physics Division, Hanscom Air Force Base.

Luvall, J.C. 1988. Using the TIMS to estimate evapotranspiration from a white pine forest. In *Remote Sensing for Resource Inventory, Planning and Monitoring*, ed. J.D. Greer, pp. 90–98. Falls Church, Va.: American Society for Photogrammetry and Remote Sensing.

Luvall, J.C., and Holbo, H.R. 1989. Measurement of short-term thermal responses of coniferous forest canopies using thermal scanner data. *Remote Sensing of Environment* 27:1–10.

Miller, D.R. 1975. Microclimate at an oak forest–asphalt parking lot interface. In *Proceedings of the 12th Conference on Agricultural and Forest Meteorology*, pp. 35–36. Tucson, Arizona, April 14–16, 1975, American Meteorological Society.

Monteith, J.L. 1973. *Principles of Environmental Physics*. London: Edward Arnold.

Nieuwenhuis, G.J.A.; Schmidt, E.H.; and Thunnissen, H.A.M. 1985. Estimation of regional evapotranspiration of arable crops from thermal infrared images. *International Journal of Remote Sensing* 6:1319–34.

Oke, T.R. 1987. *Boundary Layer Climates*. New York: John Wiley and Sons.

Palluconi, F.D., and Meeks, G.R. 1985. Thermal Infrared Multispectral Scanner (TIMS): an investigator's guide to TIMS data. Jet Propulsion Laboratory Publication 85–32.

Pelletier, R.E. 1985. Identification of linear features in agricultural landscapes through spatial analysis of thermal infrared multispectral data. In *Proceedings Technical Papers American Society Photogrammetry*, pp. 381–90. Washington, D.C., March 10–15, 1985.

Pelletier, R.E.; Ochoa, M.C.; and Hajek, B.F. 1985. Agricultural applications for thermal infrared multispectral scanner data. In *Proceedings 11th International Symposium Mach. Process. of Remotely Sensed Data*, pp. 321–28. West Lafayette, Ind., June 25–27, 1985.

Pierce, L.L., and Congalton, R.G. 1988. A methodology for mapping forest latent heat flux densities using remote sensing. *Remote Sensing of Environment* 24:405–18.

Press, W.H.; Flannery, B.P.; Teulosky, S.A.; and Vetterling, W.T. 1986. *Numerical Recipes*. Cambridge: Cambridge University Press.

Quattrochi, D.A., and Rowntree, R.A. 1988. Potential of thermal infrared multispectral scanner (TIMS) data for measurement of urban vegetation characteristics. In *Remote Sensing for Resource Inventory, Planning and Monitoring*, ed. J.D. Greer, pp. 344–51. Falls Church, Va.: American Society for Photogrammetry and Remote Sensing.

Ranney, J.W.; Bruner, M.C.; and Levenson, J.B. 1981. The importance of edge in the structure and dynamics of forest islands. In *Forest Island Dynamics in Man-Dominated Landscapes*, eds. R.L. Burgess and D.M. Sharpe, pp. 67–95. New York: Springer-Verlag.

Reginato, R.J.; Jackson, R.D.; and Pinter, P.J., Jr. 1985. Evapotranspiration calculated from remote multispectral and ground station meteorological data. *Remote Sensing of Environment* 18:75–89.

Risser, P.G. 1987. Landscape ecology: state of the art. In *Landscape Heterogeneity and Disturbance*, ed. M.G. Turner, pp. 3–14. New York: Springer-Verlag.

Seguin, B., and Itier, B. 1983. Using midday surface temperature to estimate daily evaporation from satellite thermal IR data. *International Journal of Remote Sensing* 4:371–83.

Selby, S.M., ed. 1968. *Standard Mathematical Tables*. 16th ed. Cleveland, Ohio: Chemical Rubber Co.

Shannon, C.E. 1949. Communication in the presence of noise. *Proceedings of the IRE*37:10–21.

Soer, G.J.R. 1980. Estimation of regional evapotranspiration and soil moisture conditions using remotely sensed crop surface temperatures. *Remote Sensing of Environment* 9:27–45.

Stone, L.R., and Horton, M.L. 1974. Estimating evapotranspiration using canopy temperatures: field evaluation. *Agronomy Journal* 66:450–54.

Sweat, M., and Carroll, J.E. 1983. On the use of spectral radiance models to obtain irradiances on surfaces of arbitrary orientation. *Solar Energy* 30(4):373–77.

Thistle, H.W.; Miller, D.R.; and Lin, J.D. 1987. Turbulent flow characteristics at the edge of a foliated and unfoliated deciduous canopy. In *Proceedings of the 18th Conference on Agricultural and Forest Meteorology*, pp. 179–80. West Lafayette, Ind., Sept. 15–18, 1987.

Vanderwaal, J.A., and Holbo, H.R. 1984. Needle-air temperature differences of Douglas-fir seedlings and relation to microlimate. *Forest Science* 30:635–44.

Wilson, S.B., and Anderson, J.M. 1986. The applicability of LOWTRAN 5 computer code to aerial thermographic data correction. *International Journal of Remote Sensing* 7:379–88.

Reprinted from

Ecological Studies, Volume 82

Monica G. Turner Robert H. Gardner
Editors

Quantitative Methods in Landscape Ecology

The Analysis and Interpretation of Landscape Heterogeneity

Springer-Verlag
New York Berlin Heidelberg London
Paris Tokyo Hong Kong Barcelona

Reprinted from

Ecological Studies, Volume 82

Monica G. Turner Robert H. Gardner
Editors

Quantitative Methods in Landscape Ecology

The Analysis and Interpretation of Landscape Heterogeneity

Printed in the United States of America.

Springer-Verlag
New York Berlin Heidelberg London
Paris Tokyo Hong Kong Barcelona